Original scientific paper
https://doi.org/10.33180/InfMIDEM2025.303

Informacije MIDEM
Journal of Microelectronics, Electronic Components and Materials
Vol. 55, No. 3(2025), XX – XX

An Air-gapped Cavity Filter Based on MEMS Process for 5G Millimeter Wave Applications

Yan Ding[1], Jian Ding[2], Xing Fan[1], Jiayi Wang[3], Yunchun Yang[4]
[1]School of Electronic and Information Engineering, North China Institute of Science of Science and Technology, East Beijing, China
[2]National Astronomical Observatories, Chinese Academy of Sciences, Beijing, China
[3]School of Computer Science and Engineering, Guilin University of Technology, Guilin, China
[4]Silex Microsystems Technology Co., Ltd., Beijing, China

Abstract: This article presents a 5G millimeter Wave bandpass filter using air-gapped structure, which is fabricated through high-precision micro electromechanical system (MEMS) process. The grounded and open stub lines, as well as impedance transformation stub lines, which generating four transmission poles (TPs) and two transmission zeros (TZs), are proposed to achieve the design goal. Four TPs support a 24.25-27.5-GHz passband, while two TZs provide a sharp out-of-band rejection. Step-to-step design process is given to guide the 24.25-27.5-GHz bandpass filter design. The 24.25-27.5-GHz bandpass filter is fabricated and measured, which has a minimum insertion loss of 0.9dB within the passband.

Keywords: Millimeter Wave ; Bandpass filter ; Micro Electromechanical System (MEMS) ; Insertion loss

Zračni votlinski filter na MEMS osnovi za 5G aplikacije

Izvleček: V članku je predstavljen pasovni filter 5G za milimetrske valove, ki uporablja strukturo z zračnimi kapami in je izdelan z visoko natančnim postopkom mikroelektromehanskega sistema (MEMS). Za dosego cilja zasnove so predlagani ozemljeni in odprti kraki ter kraki s transformacijo impedance, ki ustvarjajo štiri prenosne pole (TP) in dve prenosni ničli (TZ). Štirje TP podpirajo prepustni pas 24,25-27,5 GHz, dva TZ pa zagotavljata zavrnitev izven frekvenčnega pasu. Podan je postopek načrtovanja 24,25-27,5-GHz prepustnega pasu. Izdelan in izmerjen je 24,25-27,5-GHz pasovni filter, ki ima najmanjšo izgubo 0,9 dB znotraj prepustnega pasu.

Ključne besede: Milimetrsko valovanje ; Pasovni filter ; Mikroelektromehanski sistem (MEMS) ; Vložna izguba

** Corresponding Author's e-mail: jilia.123@163.com*

1 Introduction

Millimeter wave bandpass filter as one of the important circuit blocks in 5G wireless communication system has attracted great attention in recent years. Most of reported bandpass filter are designed by planar transmission lines based on printed circuit board (PCB) [1], [2]. Some researchers use some new technologies, such as the substrate integrated waveguide (SIW) in [3], integrated passive devices (IPD) in [4], and the low-temperature co-fired ceramic (LTCC) in [5], to design high-performance bandpass filters. However, traditional substrate-based PCB, SIW, IPD, and LTCC technologies suffer from high loss that associated with dielectric loss, especially at mm-wave frequency.

With the rapid expansion of 5G millimeter wave wireless communication system, extensive studies have been attracted on the structures presenting the lowest loss. The recta-coax is a 3-D transmission structure which is completely shielded and has air-gapped cavity, allowing for wideband, low loss, and high-power handling capacity [6]. The low-loss phase shifter with wide tunable range in [7], the 8-40GHz broadband integrated antenna array in [8], and the ultra-compact G-band 16-way power splitter/combiner with low insertion loss in [9] exhibits the great advantages of the air-gapped recta-coax structure.

The aim of this paper is to design and fabricate an air-gapped cavity bandpass filter for 5G millimeter wave frequency bands. The frequency response of the filter can be customed by controlling TPs and TZs. The proposed air-gapped cavity filter is excited by ground-signal-ground (GSG) probe pad [10] which allow the on-chip measurement and easy integration with planar circuits. The implemented bandpass filter exhibits the characteristics of wide bandwidth and low insertion loss. The detailed design and discussion are given in the following texts.

2 Design and Simulation

The schematic of proposed bandpass filter can be given by Fig. 1.

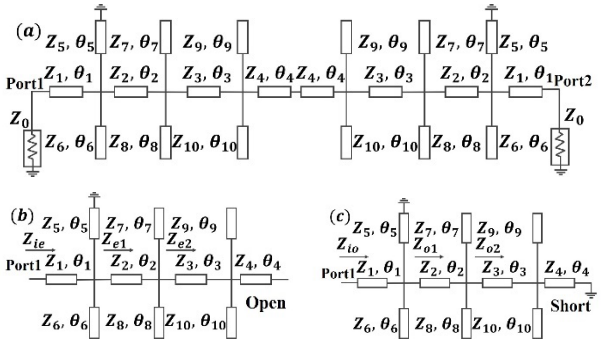

Figure 1: (a)schematic diagram of proposed bandpass filter (b) equivalent even-mode circuit (c) equivalent odd-mode circuit.

Z_i and θ_i are the characteristic impedance and electrical length of stub lines. The open stubs (i = 6,7,8,9,10) and ground stubs (i = 5), as well as impedance transformation lines (i = 1,2,3,4) are employed to obtain multiple resonant points and desired bandwidth. The equivalent even and odd mode circuits are used to analyze the structure, and the input impedance Z_{ie}, Z_{io} can be derived as:

$$Z_{ie} = Z_1 \frac{(Z_{e1} \| \frac{Z_6}{j\tan(\theta_6)} \| jZ_5\tan(\theta_5)) + jZ_1\tan(\theta_1)}{Z_1 + j(Z_{e1} \| \frac{Z_6}{j\tan(\theta_6)} \| jZ_5\tan(\theta_5))\tan(\theta_1)} \quad (1)$$

$$Z_{io} = Z_1 \frac{(Z_{o1} \| \frac{Z_6}{j\tan(\theta_6)} \| jZ_5\tan(\theta_5)) + jZ_1\tan(\theta_1)}{Z_1 + j(Z_{o1} \| \frac{Z_6}{j\tan(\theta_6)} \| jZ_5\tan(\theta_5))\tan(\theta_1)} \quad (2)$$

Where Z_{e1} can be represented by Z_{e2}, Z_i and θ_i (i = 2,7,8), and Z_{e2} can be represented by Z_i and θ_i (i = 3,4,9,10), so as the Z_{o1} and Z_{o2}.

The S parameters of the two-port network can be represented as [11]:

$$S_{12} = S_{21} = \frac{Z_0(Z_{ie} - Z_{io})}{(Z_0 + Z_{ie})(Z_0 + Z_{io})} \quad (3)$$

$$S_{11} = S_{22} = \frac{(Z_{ie}Z_{io} - Z_0^2)}{(Z_0 + Z_{ie})(Z_0 + Z_{io})} \quad (4)$$

The impedance at the port can be derived for impedance invariance property of the grounded stub line (Z_5, θ_5), and it can be expressed as:

$$Z_{in} = Z_5 \frac{0 + jZ_5\tan(\theta_5)}{Z_5 + j*0*\tan(\theta_5)} = jZ_5 \tan\left(\frac{\pi}{2}\frac{f}{f_0}\right) \quad (5)$$

Z_{in} equals to 0 at frequency 0 and $2f_0$, which contribute TZs out-of-band. According to Eq. (3), when $Z_{ie} = Z_{io}$, $S_{12} = S_{21} = 0$, and the remaining TZs can be solved. The frequency points of TPs can be derived by $Z_{ie} = Z_{io} = 0$. However, it is hard to solve complex analytic equations, so we used EDA software for research. The initial length of the stub lines is fixed at f_0, and is set as quarter-wavelength. The TPs and TZs can be adjusted by Z_i and θ_i, good in-band return loss and bandwidth are finally obtained by appropriate parameters. Fig. 2 shows the distribution of TPs from 15GHz to 35GHz. It can be seen that three even TPs and four odd TPs are generated. TPs with frequencies below 20 GHz are significantly outside the intended design frequency range and they are difficult to adjust into the band, so the three TPs are ignored. The corresponding frequency response is shown in Fig. 3. The 24.25-27.5-GHz bandwidth is obtained, and the out-of-band rejection is better than 30dB at 22GHz and 30GHz. The return loss within band is near 20dB and there are four poles in the band.

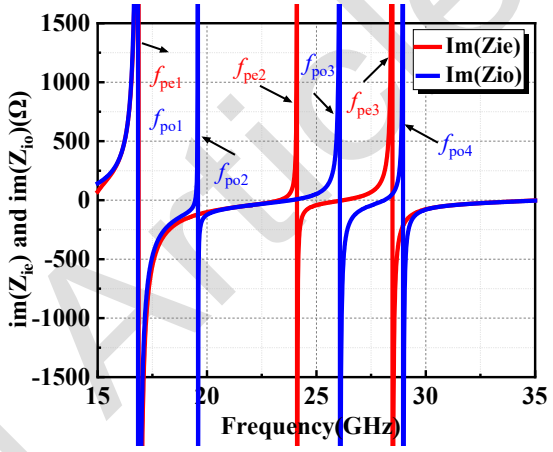

Figure 2: Distribution of TPs from 15GHz to 35GHz.

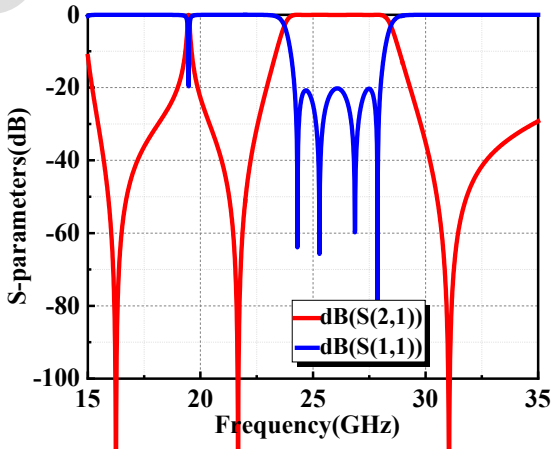

Figure 3: Frequency response corresponding to fig. 2.

Fig. 2 and Fig. 3 are the simulation results based on ideal transmission lines. In order to reflect the effects of actual physical structures, such as parasitic parameters and coupling effects, 3D model using air-gapped recta-coax is built in high frequency structure simulator. Fig. 4 shows the cross-section of five-layers recta-coax. The outer conductor and inner conductor are made by copper with height of 50 μm for each layer. The height of inner conductor is 34 μm for it is supported by a dielectric strap with a relative permittivity ε_r about 3.2 with a height of 16 μm. The outer section is 750 μm by 250 μm, while the inner section is 500 μm by 150 μm. With the thickness of each layer increases, the range of

impedance changes is wider, but the process complexity also increases. The 50 μm thickness of each layer is chosen to facilitate the realization of proposed filter. The line is highly isolated, as the outer conductor is a natural shield for the field contained within the transmission line. The 750μm periodic release holes and dielectric support straps are arranged and have been proved by previous experiments to release photoresist effectively and provide enough mechanical strength strongly. The size of release hole is 300 μm ×240 μm, and the width of dielectric support strap is 150 μm.

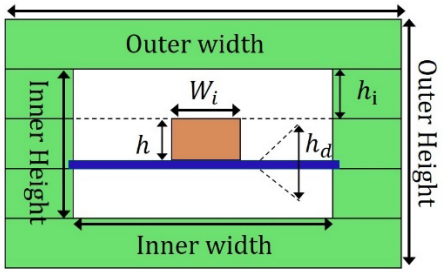

Figure 4: Cross-section of 5 layers recta-coax.

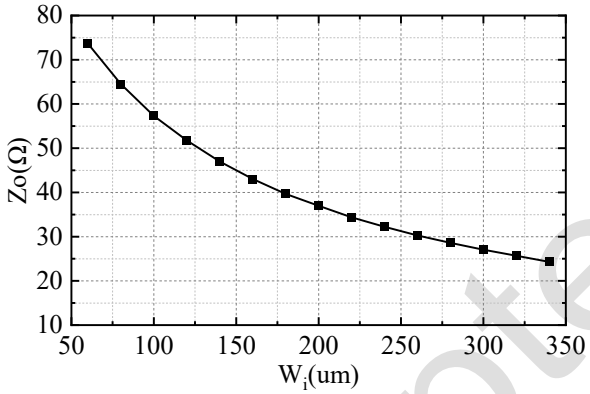

Figure 5: Simulated possible characteristic impedance with different W_i.

The physical lengths of full waveguide length at the desired frequency f_0 can be achieved by c/f_0. Different characteristic impedances are obtained by different W_i, and the range of possible characteristic impedances is shown in fig. 5. The initial length and width of the proposed 3D air-gapped filter using recta-coax are set according to the ideal values obtained in EDA software. The physical dimensions are optimized by finite element simulation, considering discontinuities and parasitic effects.

Fig. 6 shows the 3D view and the electric field of the 24.25-27.5-GHz bandpass filter. In order to reduce the total size of the filter, the feeder of input port and output port are bent by 90 degrees. The release holes, dielectric support straps, and GSG transitions are then added to fig. 6 to participate in optimization. The finally optimized physical dimensions of proposed 24.25-27.5-GHz bandpass filter are shown in Table 1. Fig.7 shows the finally layout of the proposed 24.25-27.5-GHz bandpass filter.

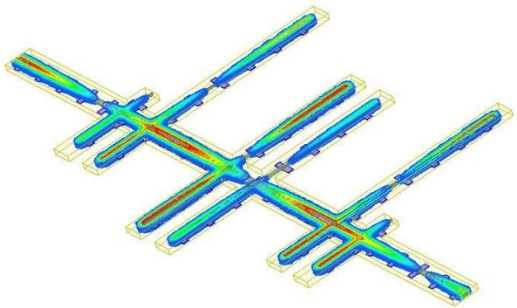

Figure 6: 3D view and the electric field of the 24.25-27.5-GHz bandpass filter.

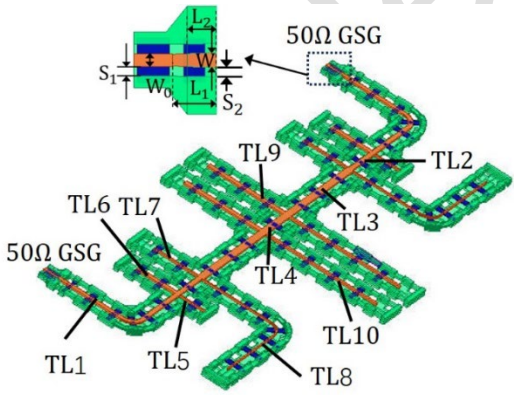

Figure 7: Layout of the proposed 24.25-27.5-GHz bandpass filter.

Table 1: Optimized physical dimensions of proposed 24.25-27.5-GHz bandpass filter (Unit: μm).

TL	Z_i, θ_i	W_i	length	GSG	
TL1	Z_1, θ_1	105	3243	W_0	90
TL2	Z_2, θ_2	118	866	W	107
TL3	Z_3, θ_3	157	2551	S_1	50
TL4	Z_4, θ_4	157	485	S_2	37.5
TL5	Z_5, θ_5	45	727	L_1	340
TL6	Z_6, θ_6	108	1178	L_2	180
TL7	Z_7, θ_7	52	1350	height	
TL8	Z_8, θ_8	36	4085	h	34
TL9	Z_9, θ_9	112	2300	h_i	50
TL10	Z_{10}, θ_{10}	68	3250	h_d	16

Fig. 8 plots the S-parameters of the proposed 24.25-27.5-GHz bandpass filter. Within the 24.25-27.5-GHz passband, the insertion loss is less than 0.7dB, and the return loss is near -20dB. The out-of-band rejection is better than 38dB at 22GHz and 30GHz.

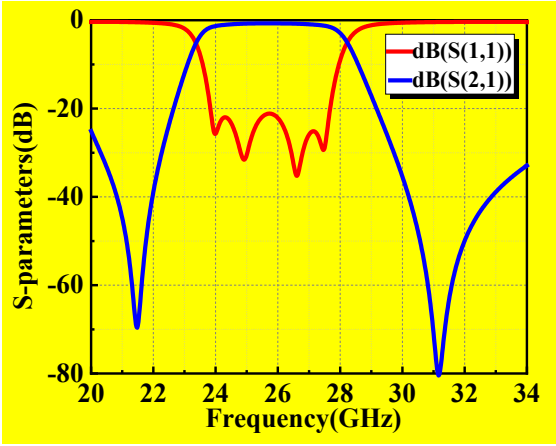

Figure 8: S-parameters of the proposed 24.25-27.5-GHz bandpass filter.

3 Fabrication and measurement

The air-gapped cavity filter is fabricated using standard MEMS processes on a silicon substrate with a thickness of 700 μm. Fig. 9 shows the detailed steps, including repeated deposition, lithography and electroplating processes. Finally, photoresist is removed through release holes, leaving a wafer filled with recta-coax.

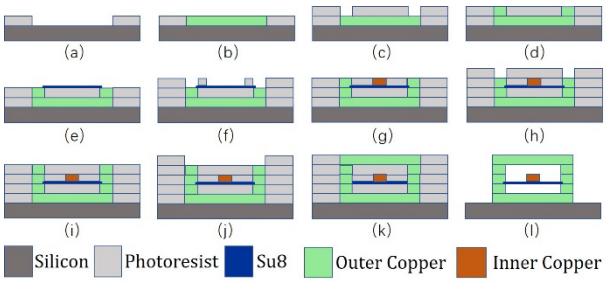

Figure 9: standard MEMS processes for recta-coax (a) lithography (b) electroplating and planarization (c) Photoresist spun and patterned (d) second copper layer is formed (e)deposition of dielectric strap (f) ~(k) repeat the previous steps (l) Photoresist is removed through release holes.

Fig. 10 shows the partial microscopic photograph of the proposed bandpass filter, and the conductors stacked on top of each other, as well as release holes can be seen clearly. The global photograph of the filter is shown in Fig. 11 with size of $9670\ \mu m \times 5550\ \mu m \times 250\ \mu m$. The filter was measured using a vector network analyzer, and the simulated and measured results are plotted for comparison in fig. 12. The measured center frequency is 25.875GHz with fractional bandwidth (FBW) of 12.5%, and a frequency shift of 120MHz (< 0.5%) is observed between the simulated and measured results. Within 24.25-27.5-GHz bandpass, the measured minimum insertion loss is 0.9dB, which is 0.2dB larger than the simulation result. In addition, the return loss of a better sample is less than -14dB.

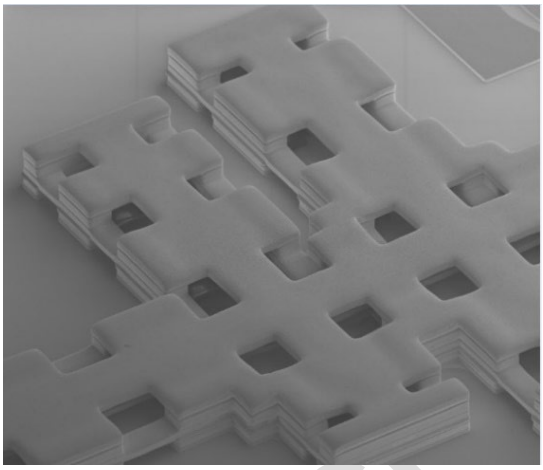

Figure 10: Partial microscopic photograph of the proposed bandpass filter.

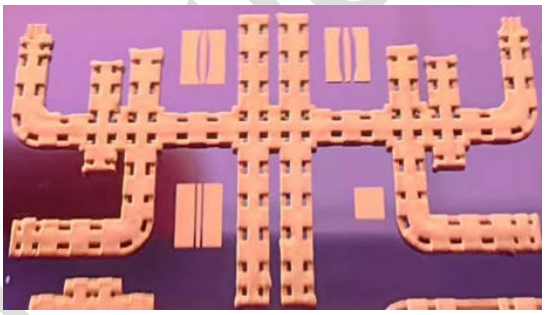

Figure 11: Photograph of the proposed filter.

The reason for differences between measured and simulated results is the inaccuracies of the manufacturing and measurement. The fabrication error includes over-etching, surface roughness, deviation of thickness. During the photoresist removal process, the etching solution might not react adequately with the photoresist, resulting in an incomplete removal. The deviations from the ideal structure mentioned above can result in changes to the equivalent capacitance or inductance of the filter structure, thereby degrading its performance. With the advancement of process technology, there is hope for further enhancing the performance of the filters.

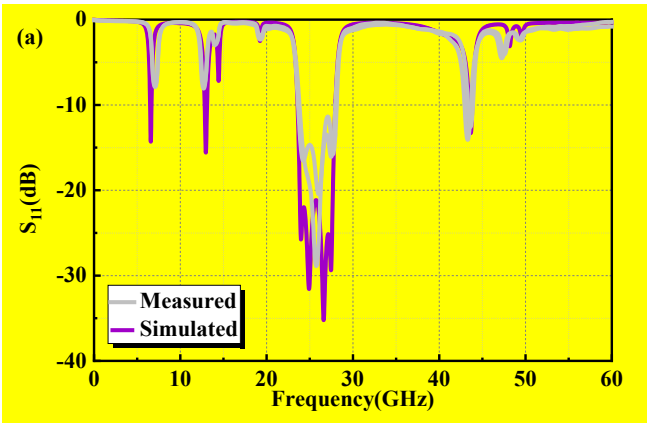

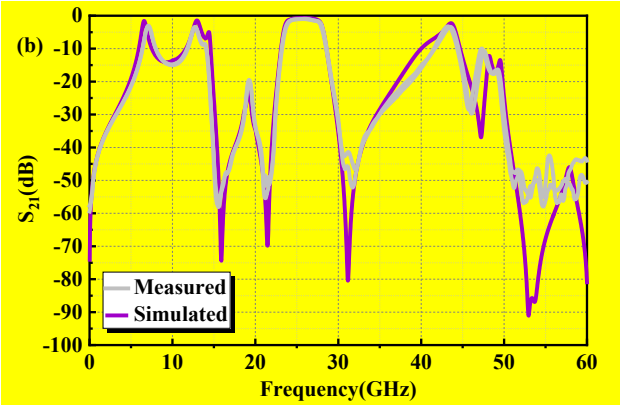

Figure 12: Measured and simulated results of the proposed filter (a) S11 (b) S21

Table 2: Performance comparison with some reported bandpass filters and proposed filters.

Ref	Form	f_0 (GHz)	FBW (%)	IL (dB)	Size mm^3
This work	Recta-coax	25.875	12.5	1.4	13
[12]	SIW (Si)	29.8	5	3.5	4
[13]	SIW (PCB)	21	1.59	1.1	4219
[14]	Recta-coax	36	0.59	2.57	16

Table 2 presents a comparison between some typical bandpass filters for 5G millimeter wave applications and the proposed structures. Filters using silicon based SIW technology in [12], has a compact structure and high selectivity, but suffer from relatively high insertion loss. The PCB-based SIW technology in [13] has mature manufacturing and low cost, but has very big footprint. Compare with recta-coax based filter in [14], a wider frequency response and lower loss have been successfully achieved. Furthermore, the 3-D air-gapped cavity enhances heat dissipation compared to planar circuits and boosts power handling capability.

4 Conclusions

A 24.25-27.5-GHz air-gapped cavity bandpass filter using MEMS process is presented in this study. Measured results show that the proposed 24.25-27.5-GHz band pass filter has the merits of low loss, wide bandwidth, and high out-of-band rejection. The proposed 24.25-27.5-GHz bandpass filter has the potential advantages in the application of the 5G millimeter wave wireless communication system, satellite communications, RF telemetry, and so on.

5 Acknowledgments

This work is supported by the Fundamental Research Funds for the Central Universities (3142025013, 3142023023).

6 Conflict of Interest

The authors declare no conflict of interest.

7 References

[1] A. Augustine and K. J. Vinoy, "A Wideband Substrate Integrated Waveguide Bandpass Filter for 5G Millimeter Wave Transceiver," *2022 IEEE Microwaves, Antennas, and Propagation Conference (MAPCON)*, Bangalore, India, 2022, pp. 1283-1286,
https://doi:10.1109/MAPCON56011.2022.10047406.

[2] Y. -C. Lin, S. -C. Lin, Y. -J. Lee and T. -Y. Huang, "Millimeter-Wave Bandpass Filter on Printed Circuit Board with Conventional Microstrip Line Structure," *2021 International Symposium on Antennas and Propagation (ISAP)*, Taipei, Taiwan, 2021, pp. 1-2,
https://doi: 10.23919/ISAP47258.2021.9614477.

[3] X. Zhou, G. Zhang, J. Zheng, W. Tang and J. Yang, "SIW Filter With Adjustable Number of Passbands Using Assembled Multimode Resonant PCBs," in *IEEE Transactions on Circuits and Systems II: Express Briefs*, vol. 69, no. 8, pp. 3386-3389, Aug. 2022,
https://doi: 10.1109/TCSII.2022.3157713.

[4] M. Ali *et al.*, "First Demonstration of Compact, Ultra-Thin Low-Pass and Bandpass Filters for 5G Small-Cell Applications," in *IEEE Microwave and Wireless Components Letters*, vol. 28, no. 12, pp. 1110-1112, Dec. 2018,
https://doi: 10.1109/LMWC.2018.2876769. .

[5] T. Martin, A. Ghiotto, T. -P. Vuong and F. Lotz, "Self-Temperature-Compensated Air-Filled Substrate-Integrated Waveguide Cavities and Filters," in *IEEE Transactions on Microwave Theory and Techniques*, vol. 66, no. 8, pp. 3611-3621, Aug. 2018,
https://doi: 10.1109/TMTT.2018.2851243.

[6] F. David, M. Chatras, C. Dalmay, L. Lapierre, L. Carpentier and P. Blondy, "Surface-Micromachined Rectangular Micro-Coaxial Lines for Sub-Millimeter-Wave Applications," in *IEEE Microwave and Wireless Components Letters*, vol. 26, no. 10, pp. 756-758, Oct. 2016,
https://doi: 10.1109/LMWC.2016.2604867.

[7] Olusegun Sholiyi and John D. Williams. "Microrectangular-coaxial phase shifter for microwave devices," Int. J. RF Microw. Comput.-Aided Eng. 25, 6 (August 2015), 502–509. https://doi.org/10.1002/mmce.20885

[8] Vanhille K , Durham T , Stacy W ,et al. "A Microfabricated 8-40 GHz Dual-Polarized Reflector Feed," [Online]. Available: http://ntrs.nasa.gov. [Accessed: 20-Oct-2018].

[9] H. Kazemi *et al*., "Ultra-compact G-band 16way power splitter/combiner module fabricated through a new method of 3D-copper additive manufacturing," *2015 IEEE MTT-S International Microwave Symposium*, Phoenix, AZ, USA, 2015, pp. 1-3,
https://doi: 10.1109/MWSYM.2015.7166718.

[10] Ding Y, et al.: "Design and comprehensive analysis of a novel structure of ARCL-to-SCL GSG transition for millimeter wave applications," IEICE Electron, , vol. 20, , no. 3, pp. 20220526,2023, https://doi: 10.1587/elex.19.20220526

[11] Pozar D M. Microwave engineering. Fourth Editions. University of Massachusetts at Amherst, John Wiley & Sons, Inc, 2012, pp. 328-333.

[12] T. Martin, A. Ghiotto, T. -P. Vuong and F. Lotz, "Self-Temperature-Compensated Air-Filled Substrate-Integrated Waveguide Cavities and Filters," in *IEEE Transactions on Microwave Theory and Techniques*, vol. 66, no. 8, pp. 3611-3621, Aug. 2018,
https://doi: 10.1109/TMTT.2018.2851243.

[13] Zhu H , Li J , Cao L ,et al, "Si-Based Ka-band SIW Band-pass Filter using Wafer Level Manufacturing Process," Institute of Electronics, Information and Communications Engineers (IEICE), 2021(1).
https://DOI:10.1587/ELEX.17.20200414.

[14] Reid J R , Oliver J M , Vanhille K ,et al, "Three dimensional metal micromachining: A disruptive technology for millimeter-wave filters," IEEE, 2012.
https://DOI:10.1109/SiRF.2012.6160165.

Arrived: 29.11.2024
Accepted: 04.04.2025